Colloids and Surfaces B: Biointerfaces 226 (2023) 113301

Contents lists available at ScienceDirect

Colloids and Surfaces B: Biointerfaces

journal homepage: www.elsevier.com/locate/colsurfb

Synthesis and characterization of lipopolysaccharide (LPS) anchored polystyrene microparticles as a synthetic model system for attachment studies

Jan David Schutter [a], Karl Eberhardt [a], Anna Maria Elert [a], Jörg Radnik [a], Daniel Geißler [a,b], Ozlem Ozcan [a,*]

[a] Bundesanstalt für Materialforschung und -prüfung (BAM), Unter den Eichen 87, 12205 Berlin, Germany
[b] PolyAn GmbH, Schkopauer Ring 6, 12681 Berlin, Germany

ARTICLE INFO

Keywords:
Bacterial lipopolysaccharides
Pseudomonas aeruginosa
Polystyrene microparticles
Swell-capture
Biomimicryc

ABSTRACT

Outer membrane lipopolysaccharides (LPS) play a crucial role in determining attachment behavior and pathogenicity of bacteria. The aim of this study was to develop a simple procedure for anchoring bacterial lipopolysaccharides to polystyrene (PS) microparticles as a model system for in situ attachment studies. By using a swell-capture methodology, commercially available LPS of *Pseudomonas aeruginosa* (strain ATCC 27316 serotype 10.22) was anchored onto PS microparticles in a proof-of-concept study. A detailed chemical and morphological characterization has proven the success of LPS incorporation. It was shown that the coverage and structure of the LPS film was concentration dependent. The procedure can easily be adapted to LPS of other bacterial strains to generate a synthetic model toolkit for attachment studies.

1. Introduction

Outer membrane structure and chemistry govern many medically and technically important properties of microorganisms such as their pathogenicity and ability to attach to abiotic surfaces [1–3]. The outer membrane of Gram-negative bacteria is a bilayer. The inner leaflet consists of phospholipids whereas the main components of the outer leaflet are lipopolysaccharides (LPS) [5]. One LPS molecule consists of three domains: the lipid A, the core oligosaccharide, and the O-antigen. The hydrophobic lipid A anchors the LPS into the membrane. The core oligosaccharide links the lipid A to the O-antigen, which protrudes into the medium. The O-antigens are built up from oligosaccharides of 1–8 sugars. Often the linear or branched (O-antigen) structures contain substituents like phosphate groups, acetyl groups, glycerol, etc. [6]. The O-antigen of P. aeruginosa serotype 10 is build up on repeating units of N-acetylgalactosaminuronic acid (GalNA), N-Acetyl-D-Quinovosamine (QuiN) and rhamnose (Rha) [7]. Due to their uniqueness, LPS can be used in serological diagnostic tests [8], either to detect antibodies formed by an immune response or conversely to be diagnosed by antibodies [9].

The first attachment of bacteria on a surface required to initiate the biofilm formation is governed by chemical and electrochemical cell-substrate interactions which involves cell appendages (such as pili and/or fimbriae) and LPS [10]. For the design of synthetic model systems mimicking bacteria to be used in attachment studies, targeting the LPS-controlled reversible processes is more applicable, as the molecular chemistry of LPS can be better characterized and controlled than the cell adhesins and appendages. Moreover, this approach shall directly enable systematic studies on effects of environmental variables on LPS configuration and chemistry, as well as the resulting attachment characteristics [11–14].

LPS extracted from bacteria has already been incorporated into particles and particle surfaces in many studies, primarily for medical applications. It was embedded in poly(D,L-lactide-co-glycolide) microparticles [15] and in nano- and microparticles of poly(lactic-co-glycolic acid) [16]. The adsorption of LPS on the particles was demonstrated for latex microbeads [17], polystyrene sulfonate nanoparticles [18], carboxylated and PEGylated polystyrene nanoparticles [19], Gantrez® nanoparticles [20] and immunomagnetic microbeads [21]. A reusable system for adsorption and desorption of LPS by alkanethiol coated Fe_3O_4/Au/Fe_3O_4 magnetic core-shell nanoparticles was established by Prasad et al. [22]. Magnetic nanoparticles were also used by Piazza et al.

* Corresponding author.
E-mail address: ozlem.ozcan@bam.de (O. Ozcan).

https://doi.org/10.1016/j.colsurfb.2023.113301
Received 3 June 2022; Received in revised form 4 March 2023; Accepted 5 April 2023
Available online 7 April 2023

[23], where LPS was anchored by a hydrophobic brush of oleylamine. Furthermore, polyallylamine hydrochloride was used to link LPS to alginate-coated chitosan nanoparticles [24] and CuS nanoparticles [25] in previous reports.

The aim of this study was to develop a novel, linker-free method for attaching LPS molecules to polymer microparticles by means of a swell-capture method. The swell-capture method has originally been developed to sterically incorporate hydrophobic fluorescent dyes into polymer particles [26,27]. We adapted this concept to LPS of *P. aeruginosa* to incorporate the LPS molecules into the outmost surface of PS microparticles. The chemistry, surface charge and morphology of the particles were characterized by means of X-ray photoelectron spectroscopy (XPS), atomic force microscopy (AFM)-based infrared spectroscopy (AFM-IR), ζ-potential measurements and AFM-topography analysis. The presented methodology for grafting LPS onto PS microparticles is the first step in developing a synthetic model system for bacterial attachment studies and could be useful in the design of new diagnostic platforms.

2. Material and methods

2.1. Materials

Plain 1 μm diameter PS microparticles (2.5%) were purchased from Kisker Biotech (Steinfurt, Germany). Phenol extracted lipopolysaccharides from *P. aeruginosa* (strain ATCC 27316 serotype 10.22) and fluorescein-5(6)-isothiocyanate (FITC) were purchased from Sigma Aldrich (Steinheim, Germany). Borate buffer (pH 10.00), tetrahydrofuran (THF), ethanol, PBS buffer (pH 7.4), NH_3 (30%) and H_2O_2 (25%) were acquired from Chemsolute (Th. Geyer, Berlin, Germany). Mica sheets (V1 quality, 0.16 mm thickness) were procured from Plano GmbH (Wetzlar, Germany). Epoxy adhesive epo-tek 377 was purchased from Epoxy Technology Inc. (Billerica, Massachusetts, U.S).

2.2. Preparation of lipopolysaccharide-coated polystyrene microparticles

The as-delivered PS microparticle dispersion and LPS solution were diluted to 10 mg/ml and 4.33 mg/ml, respectively. 100 μl of the diluted PS suspension was mixed with different volumes (12–231 μl) of the LPS solution to reach LPS concentrations of 0.07 mg/ml, 0.14 mg/ml, 0.36 mg/ml, 0.71 mg/ml, 1.07 mg/ml, 1.43 mg/ml. A PS microparticle suspension undergone the same swell-capture cycle without addition of LPS was run parallel as a zero-LPS (S0) control sample. Accordingly, the samples were designated as S1–S6 in this manuscript. After filling up with deionized water to 600 μl, 100 μl THF was added. The dispersion was shaken for 30 min at room temperature in 1.5 ml reaction tubes with a vortex-mixer (Select Vortexer, Select BioProducts, U.S.). The subsequent separation was performed by centrifugation at 5000 rcf for 5 min with a Z 206 centrifuge (Hermle Labortechnik, Wehingen, Germany), removing supernatant and refilling with deionized water. This step was performed in total three times to obtain LPS-coated PS microparticles as a suspension.

2.3. Determination of ζ-potential

For the ζ-potential measurements, 100 μl of microparticle suspensions S0–S6 and LPS solutions with the same concentrations were mixed with 900 μl of PBS (pH 7.4). The measurements were performed at 25 °C with a Zetasizer Nano ZS (Malvern Instruments Ltd, UK).

2.4. Characterization of surface chemistry

XPS measurements were performed on drop-casted samples. For this purpose, 15 μl dispersion of samples S0–S6 and untreated PS microparticle reference, was dropped on a cleaned silicon wafer and dried under vacuum. The silicon wafers were previously cleaned by immersion for 10 min in a mixture of deionized water, NH_3 and H_2O_2 (in the ratios of 5:1:1, caution: peroxide is a strong oxidizing agent, avoid contact with organic materials and solvents) at 80 °C, rinsing two times in deionized water in an ultrasonic bath and drying with N_2. Analysis was performed at least on two replicates.

X-ray photoelectron spectroscopy (XPS) measurements were performed with an AXIS Ultra DLD photoelectron spectrometer manufactured by Kratos Analytical (Manchester, UK) with monochromatic Al Kα radiation ($h\nu = 1486.6$ eV) at a pressure of approximately $5 \bullet 10^{-7}$ Pa. The electron emission angle was 0° and the source-sample-analyzer angle was 60°. The binding energy scale of the instrument was calibrated following a Kratos Analytical procedure which uses ISO 15472 binding energy data. The XPS spectra were taken by setting the instrument to the hybrid lens mode and the slot mode providing approximately a 300 × 700 μm^2 analysis area. The survey and high-resolution detail spectra were measured with pass energies of 80 eV and 20 eV, respectively. All spectra were recorded in the fixed analyzer transmission mode. Furthermore, the charge neutralizer was used. The spectra were referenced to the main C1s peak at 284.9 eV. UNIFIT 2018 was used for data analysis [28]. Peak fitting was performed with a sum of the Gaussian-Lorentzian curves with a fixed Gaussian-Lorentzian ratio and a halfwidth. The obtained fitting parameters are given with the fits. For the background subtraction, a modified Tougaard background was used. The quantification was performed with the survey spectra. Therefore, the peak areas of the main peaks after subtraction with a modified Tougaard background were normalized with the element-specific Scofield factor, the spectrometer-specific transmission function and the inelastic mean free pathways of the photoelectrons.

To obtain information on local chemistry, AFM-IR measurements were performed. For the sample preparation. 15 μl of the dispersion of samples S0–S6 was dropped on fresh mica stripped gold substrate and dried under vacuum to get areas of closely packed particles. The AFM-IR data reported in this study were obtained using a NanoIR2s (Bruker / Anasys Instruments) coupled with a multichip QCL source (MIRcat, Daylight Solutions; tunable repetition rate range of 0–500 kHz; spectral resolution of 1 cm^{-1}) covering the range from 900 cm^{-1} to 1900 cm^{-1}. An Au-coated silicon probe (tapping AFM-IR cantilever, Anasys Instruments, spring constant 1–3 nN m^{-1}) was employed.

2.5. Labeling with FITC

For the preparation of FITC-labeled LPS-coated microparticles 20 μl stock solution of 20 mg/ml FITC in ethanol was mixed with 100 μl microparticles suspension of the samples S0 and S5, and 380 μl borate buffer (0.1 M, pH 10.5) was added. The reaction tubes were placed in Thermomixer-Mixer HC (Starlab, Milton Keynes, U.K) for 3 h and rotated at 800 rpm at 37 °C. After incubation, the excess FITC was removed by centrifugation at 5000 rcf for 10 min with a MiniSpin plus centrifuge (Eppendorf, Germany), discarding of the supernatant and refilling with ethanol. This step was performed three times. Subsequently, the same procedure was repeated with deionized water. Imaging of the FITC-labeled microparticles was done with a fluorescence microscope (Leica SP8, Germany). The liquid sample was excited with an LED light source with a wavelength of 470 nm and the filter cube DFT51010 (dichroic filter: 500 nm, emission: 506–532 nm, Leica, Germany) was used for detection.

2.6. Analysis of surface topography

Freshly cleaved mica pieces were prepared according to Wagner [29]. Shortly, mica stripes were cleaved, and the inner freshly exposed layer was placed into a holder of a vacuum deposition machine (Creavac, Germany). At a pressure of 10^{-6} bar gold was deposited at 1 Å/s to a thickness of 100 nm with the thermal evaporation device. Coverslips were glued with epo-tek 377 on the gold layer and heated for 1 h at 150 °C. After cooling they were stored until use. THF was used to cleave the gold layer before the experiment. Freshly exposed gold surfaces were

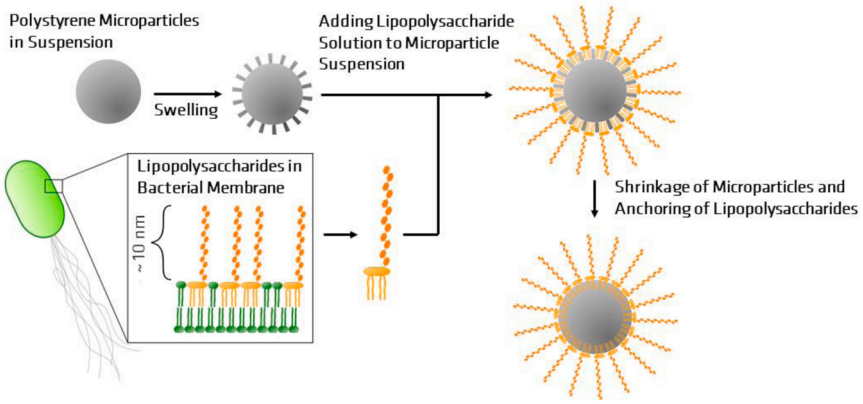

Fig. 1. Process and proposed swell-capture mechanism of preparation of LPS-coated PS microparticles. The schematics is not to the scale. PS microparticles have a diameter of 1 μm, the O-antigen has an average length of ~10 nm [4].

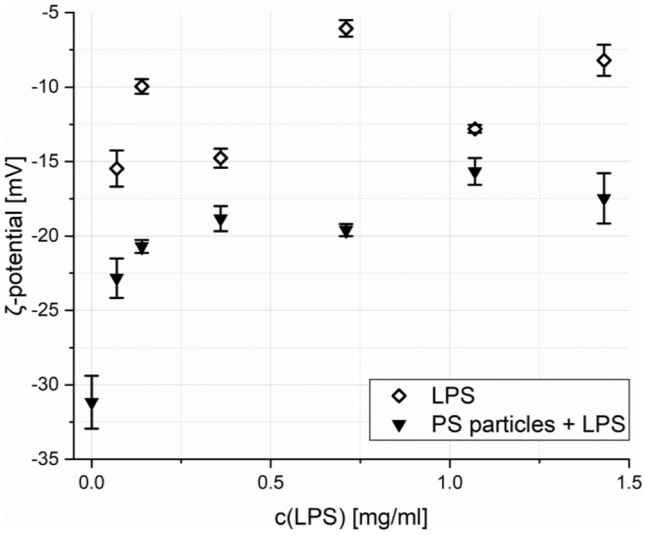

Fig. 2. ζ-potential of *P. aeruginosa* LPS at different concentrations in PBS and LPS-coated PS microparticles in PBS (pH = 7.4) as a function of the LPS concentration.

dripped with 15 μl dispersion of LPS suspension, sample S0, S5, S6 and pure PS microparticles and dried under gentle swirling in vacuum. The formation of monolayers of densely packed microparticles was observed in series of AFM images with increasing spatial resolution (the series with S6 are presented in the supplementary information Fig. S2). For the high-resolution topography analysis, AFM images were acquired in an area of 500 × 500 nm^2 and 250 × 250 nm^2 on the top surface of single microparticles within the grid to minimize artefacts due to the particle curvature. AFM measurements were performed using a Nanowizard 4 (JPK, Bruker Nano GmbH, Berlin, Germany) in higher overtone AC mode with AD-2.8-SS (Adam innovations, Ireland) cantilevers. The cantilever was vibrated at the second resonance frequency at 325.16 kHz. The calibration was performed with the thermal noise method which is implemented in the Nanowizard 4 control suite. The spring constant k_2 and the sensitivity S_2 for the second resonance frequency was 49,88 N/m and 8,2 nm/V, respectively. The power-law exponent ζ_2 according to [30] was 1.98. Scanning was performed at a line rate of 0.6 Hz with a 2 nm drive amplitude. It was crucial to use low pressure with a relative setpoint of 85–90% and a low gain. Visualization of the data was done with the software JPK Data Processing 6.1.88, it is important to note that flattening of the round sphere top leads to distortion in the topography images.

3. Results and discussion

The aim of this work was to develop a novel methodology flexibly applicable to the design of synthetic model microparticles mimicking bacterial cells. For this purpose, lipopolysaccharides of *P. aeruginosa* were impregnated into the surface of PS microparticles using a swell-capture mechanism which is schematically summarized in Fig. 1.

PS microparticles loaded with six different concentrations of LPS in PBS and PS microparticles undergone the same swell-capture cycle without addition of LPS were tested by means of ζ-potential analysis. Additionally, LPS suspensions with the same concentrations were studied to investigate the ζ-potential of the LPS molecules at relevant concentrations.

LPS of *P. aeruginosa* is mainly negatively charged in the O-antigen region in comparison to other Gram-negative bacteria [4,31]. Contributing to the charge of LPS are phosphates groups in the core oligosaccharide as well as carboxylic acids and amides in the core oligosaccharide and O-antigen [7]. Pure LPS in aqueous solutions forms aggregates above a critical concentration, with their O-antigens protruding into the aqueous phase [32]. A negative ζ-potential of −12.4 mV was reported for LPS [33] which was in agreement with our results presented in Fig. 2.

The PS subjected to the swell-capture cycle without LPS (S0) had the lowest ζ-potential value (−31 mV), which can be explained with the presence of charged groups on the PS surface. Such groups can originate from residues of polymerization initiators at the ends of the polymer chains [34]. Moreover, it is reported that the preparation method of the PS particles has a significant influence on the ζ-potential [35]. With increasing LPS concentration, the ζ-potential of the microparticles increased and approached a saturation level of ca. − 16 mV as can be seen in Fig. 2, which is approaching the ζ-potential of the LPS aggregates formed under the same conditions. The increase of the ζ-potential was asymptotic with a step between S4 (0.71 mg/ml) and S5 (1.07 mg/ml). A decrease of the negative electrophoretic mobility of PS particles with increasing coverage of LPS absorbed to the particles from the aqueous phase was reported by Peula-Garcia et al. [18]. Along with the ζ-potential, the size of the microparticles was measured using dynamic light scattering. The size distributions of the starting material as well as microparticles after swell-capture cycles with and without LPS were broad. The change in particle diameter observed between samples S0–S6 was within the statistical variation of the size distribution of the pristine PS microparticles (see Supporting Information, SI).

The incorporation of the LPS onto PS microparticles was investigated by means of XPS and AFM-IR. The atomic concentration of nitrogen, derived from the N 1 s peak at ~ 400.2 eV was used to evaluate LPS presence on the surface of the PS microparticles. Since the information comes directly from the outer region of the microparticles and the

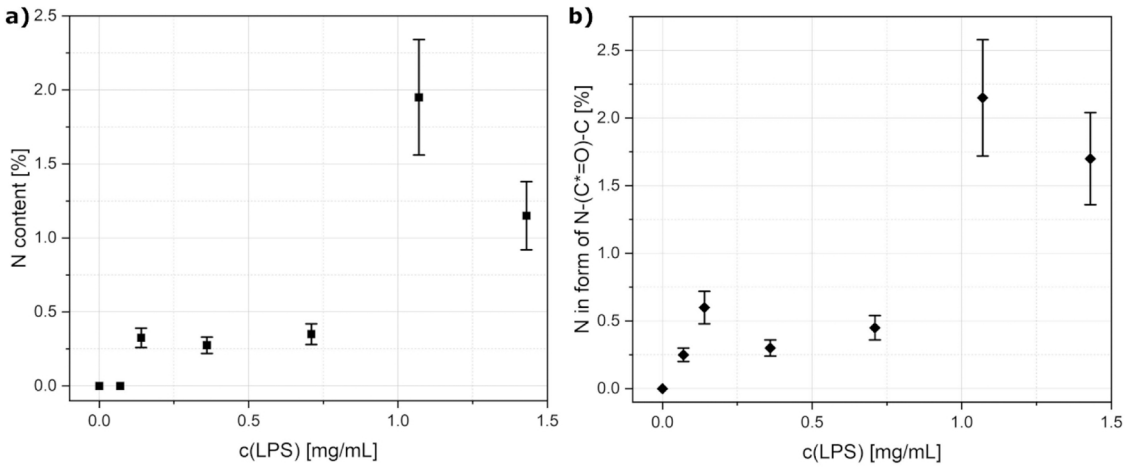

Fig. 3. Effect of LPS concentration used during particle preparation on the concentrations of nitrogen containing species analyzed by means of XPS; a) overall nitrogen concentration evaluated from the N 1 s-peak at ~ 400.2 eV; and b) the percentage of nitrogen in the form of nitrogen containing-carbon species in relation to all carbon species measured. Error bars indicate instrument-related measurement uncertainty.

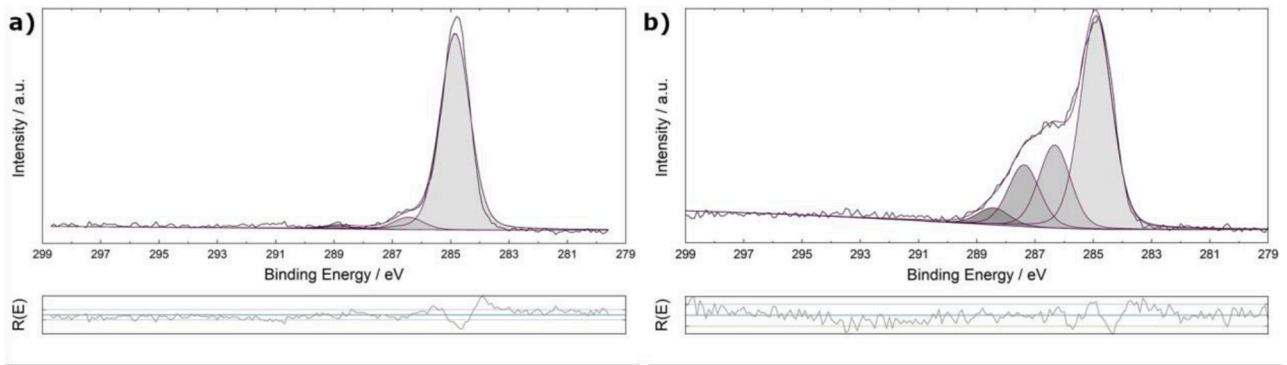

Peak name C1s_14	Peak height/ cps	Lorentzian	Position/ eV	FWHM/ eV	abs. Area/ cps·eV	rel. Area/ %
C-C, C-H	657.389	0.2	284.8522	1.2	907.34	92.28
C-OH, C-O-C	41.649	0.2	286.4436	1.2	57.59	5.86
C=O	2.46233	0.2	287.6468	1.2	3.4068	0.35
N-(C*=O)-C	10.806	0.2	288.8404	1.2	14.95	1.52

Peak name C1s	Peak height/ cps	Lorentzian	Position/ eV	FWHM/ eV	abs. Area/ cps·eV	rel. Area/ %
C-C, C-H	456.96	0.2	284.9071	1.275	674.11	56.89
C-OH, C-O-C	177.541	0.2	286.3294	1.275	261.96	22.11
C=O	132.156	0.2	287.3823	1.275	195	16.46
N-(C*=O)-C	36.563	0.2	288.4294	1.275	53.95	4.55

Fig. 4. High resolution XPS spectra of the C 1 s peak for samples S0 (a) and S5 (b) with fitting parameters of the respective species.

nitrogen originates only from the LPS molecules, the nitrogen concentration correlates directly with the coverage of LPS on the microparticles. The average measured nitrogen percentage of each sample was taken and plotted in Fig. 3a. With the S1 sample no nitrogen species were detected. The step from S4 to S5 was more pronounced. Phosphate, also a component of LPS, was not detectable since the P 2p region overlapped with the Si 2p and 2 s regions originating from the silicon wafer.

The carbon peak around 285 eV in the XPS spectra is a convolution of peaks resulting from different carbon species. The species concentration of the N-(C*=O)-C compound (peak area(N-(C*=O)-C): total C 1 s area) at around ~ 288.5 eV [36] is presented in Fig. 3b for S0–S6. Regarding the fluctuating values at the low LPS concentrations, it is noted that at lower concentrations the signal to noise ratio was quite high. Therefore, the nitrogen shoulder can only be clearly identified at values > 1 mg/ml LPS. From the results in Fig. 3, it can be concluded that the LPS occupancy follows a stepwise mechanism: at first, only traces of nitrogen from LPS are detectable on the microparticles, from ~ 1 mg/ml onwards the peaks assigned to LPS occupancy increases abruptly.

Fig. 4 shows the detail spectrum of carbon peaks for S0 (a) and S5 (b), respectively. With increasing LPS concentration, nitrogen carbon compounds become clearly visible in the spectrum. They can be attributed to amides in the LPS structure. Simultaneously, the amount of the oxygen-

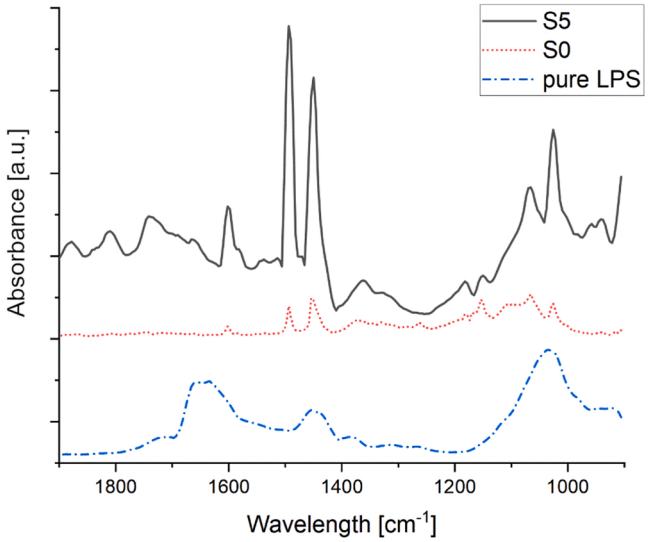

Fig. 5. AFM-IR spectra of sample S5, PS microparticles undergone the same swell-capture cycle without addition of LPS (S0) and pure LPS on Au substrates.

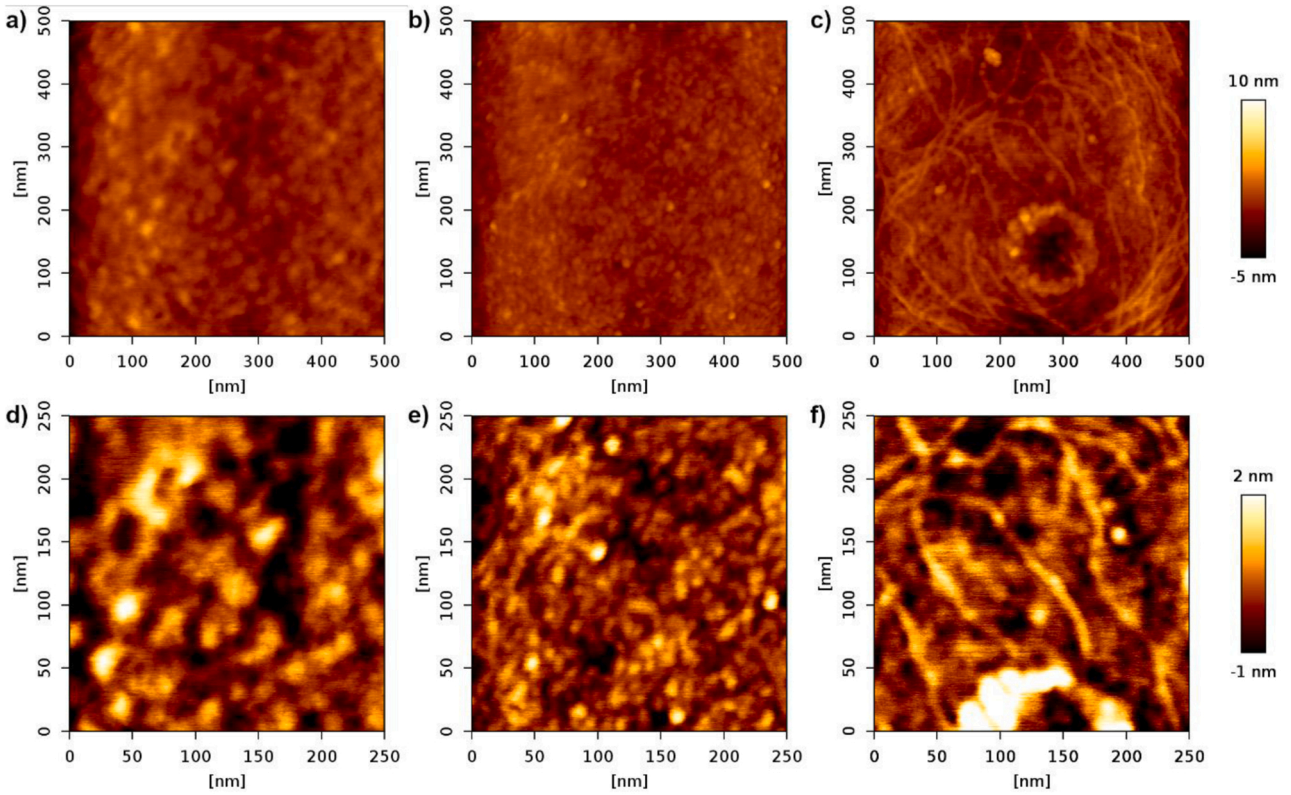

Fig. 6. AFM height measurements of (a, d) untreated PS microparticles, (b, e) microparticles undergone the same swell-capture cycle without addition of LPS (S0) and (c, f) microparticles with the highest LPS concentration (S5). High-resolution scans were performed on top of the microparticles to minimize tilt-correction induced artefacts.

containing carbon compounds attributed to sugars in the saccharide chains increased with increasing LPS concentration.

XPS analysis provides averaged chemical information from a large (~ 1 mm × 3 mm) sample area. Thus, as a second method with high spatial resolution, AFM-IR, was used to interrogate the surface chemistry of the LPS-anchored PS microparticles.

AFM-IR is a hybrid technique where chemical characterization provided by infrared spectroscopy can be obtained at the spatial resolution of AFM [37,38]. This is realized by using the gold-coated tip of AFM to locally detect thermal expansion of a sample resulting from local absorption of IR radiation. Therefore, the AFM cantilever acts in this method as the IR detector, allowing the AFM-IR technique to overcome the spatial resolution limits of conventional IR microscopy. A tunable infrared laser working in the range between 900 and 1900 cm^{-1} was applied as the source of IR radiation. Local IR spectra (Fig. 5) were collected from the pure LPS (spin-coated on gold), PS microparticles undergone the same swell-capture cycle without addition of LPS (S0), and PS microparticle with anchored LPS (S5). It should be noted that the penetration depth of the laser is much higher than the thickness of the LPS (10 – 12 nm [4]) therefore the underlaying PS in the S5 sample is also active and PS typical peaks are likewise detected by this method. Typically, LPS spectra contain a broad and relatively large peak in the carbohydrate region assigned to C-O and C-O-C vibration at 1036 cm^{-1}. The peak at 1453 cm^{-1} assigned to C-H stretching vibration was detected. Peaks at 1560 cm^{-1} and 1633–1655 cm^{-1} corresponding to ν(C-H) + δ(C-N-H) [Amide II] and ν(C═O) [Amide I] were also detected

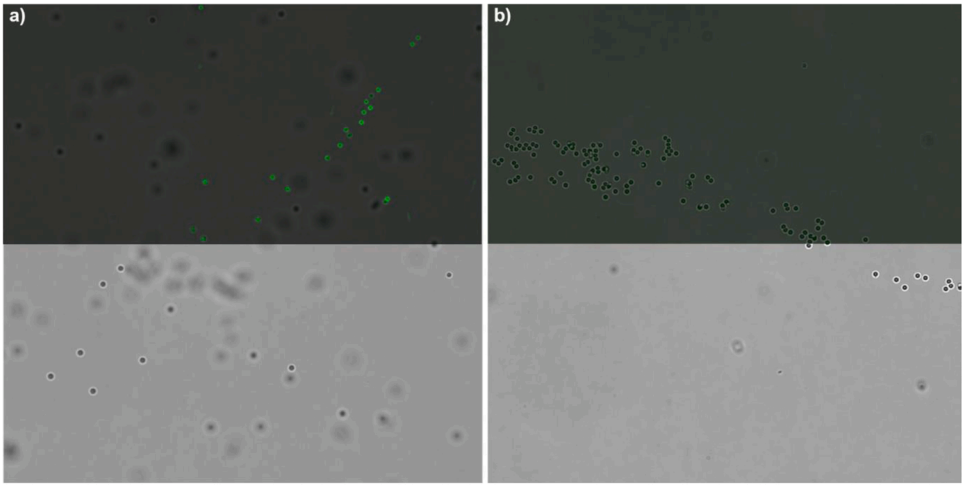

Fig. 7. Microscopy images of the LPS-coated PS particle of sample S5 (a) and the control sample S0 (b) after labeling with FITC in aqueous dispersion. Lower part is the bright-field channel and upper part is an overlay of bright-field and fluorescence channel (excitation: 470 nm LED, emission 519/25 nm bandpass filter) with 10 μm scale bar. It becomes obvious that sample S5 (with LPS) strongly emits in the FITC fluorescence channel, whereas sample S0 (without LPS) does not show significant fluorescence.

respectively [39,40]. Since those vibrations are not present in pristine PS, they were chosen as characteristic peaks to detect an attached layer of LPS on the PS microparticle. In red the spectrum of PS microparticles without LPS is presented as a comparison. In this sample typical vibration bands of PS were recorded with the double features at 1452 and 1492 cm^{-1} which are typical for vibrations of -CH_2 and benzene ring as well as a peak at 1600 cm^{-1} corresponding to C=C vibrations [41]. The appearance of LPS-specific vibrations in the AFM-IR spectra conclusively proves that the LPS anchoring was successfully achieved by means of the swell-capture method.

The AFM topography images of the as received PS microparticles as well as samples S0 and S5 are presented in Fig. 6. The monolayer of PS microparticles as well as different magnifications of S6 are presented in the SI (Fig. S2.). As seen in Fig. 6b and e, the mere treatment of PS according to the described protocol, which includes swelling with THF, influences, albeit faintly, the topography. It must be taken into account that when flattening a 3-dimensional sphere into a two-dimensional image, distortions may occur. However, small threadlike structures are visible in Fig. 6c and f which are missing on the microparticles without anchored LPS (Fig. 6a, d and b, e). Since the structures are missing on untreaded PS particles and S0 it can be assumed, that the structures in Fig. 6c and d most likely originate from the protruding LPS domains, or anchored aggregates. It should be mentioned that AFM measurements were performed in air. Hence, the presented images reflect the situation of dried LPS.

To test the homogeneity and reproducibility of the LPS anchoring process, samples S0 and S5 were labeled with FITC and imaged by means of fluorescence microscopy with irradiation at 470 nm. Fig. 7 shows microparticles of S0 and S6 which adhered to the bottom of a coverslip in aqueous suspension. The presence of FITC on the microparticles of S5 suggests covalent bonding with primary amines [42]. Such amines can be found as substitutes in the *P. aeruginosa* core oligosaccharide [43]. The strong fluorescence signal from the microparticles further assures a reproducible LPS attachment on the PS microparticles.

4. Conclusions

A simple swell-capture type procedure was developed for the attachment of LPS molecules to PS microparticles. The ζ-potential results and XPS analysis have indicated that the LPS incorporation, orientation and coverage are concentration-dependent. A shielding effect of the LPS chains on the surface charge of PS microparticles was observed in ζ-potential analysis even at the lowest LPS concentration of 0.07 mg/ml reaching stable values at 0.36 mg/ml suggesting a successful incorporation of LPS molecules on the microparticle surfaces. XPS analysis indicated that beyond LPS concentrations between ~ 0.7 mg/ml a jump in the detected LPS-specific species occurs. This might stem from an increase in packing density or attachment of LPS aggregates formed in the impregnation solution. Ongoing research focusses on the analysis of the LPS conformation by means of near ambient pressure X-Ray photoelectron spectroscopy (NAP-XPS) to limit drying induced artefacts.

AFM-IR was applied as a suitable method for obtaining chemical information at high spatial resolution. The presence of amide bands in the IR spectra of the LPS anchored microbeads provided useful evidence supporting the XPS-derived composition analysis. In the AFM topography, thread-like structures could be identified on the surface, which are assigned to patches of LPS molecules.

The simple methodology presented here can be used for the synthesis of LPS anchored microparticles as model systems for investigating the alignment and self-organization of LPS as well as for the development of attachment and immunology assays. Future studies shall focus on the detailed analysis of LPS structure and conformation as well as on the transfer of the process to LPS extracted from microorganisms with different surface properties, such as surface charge and energy.

CRediT authorship contribution statement

Jan David Schutter: Investigation, Formal analysis, Validation, Methodology, Visualization, Writing - Original Draft. **Karl Eberhardt:** Investigation, Visualization. **Anna Maria Elert**: Investigation, Formal analysis. **Jörg Radnik:** Investigation, Formal analysis. **Daniel Geißler**: Investigation, Formal analysis. **Ozlem Ozcan:** Conceptualization, Writing - Original Draft, Supervision.

Declaration of Competing Interest

The authors declare that they have no known competing financial interests or personal relationships that could have appeared to influence the work reported in this paper.

Data Availability

The raw/processed data required to reproduce these findings will be made available on request.

Acknowledgements

The authors would like to thank Frank Schreiber and Ute Resch-Genger for scientific discussions and Nithiya Nirmalananthan-Budau for assistance with the DLS measurement.

Appendix A. Supporting information

Supplementary data associated with this article can be found in the online version at doi:10.1016/j.colsurfb.2023.113301.

References

[1] S.A. Alshalchi, G.G. Anderson, Expression of the lipopolysaccharide biosynthesis gene lpxD affects biofilm formation of Pseudomonas aeruginosa, Arch. Microbiol. 197 (2015) 135–145.
[2] S.L. Walker, J.A. Redman, M. Elimelech, Role of cell surface lipopolysaccharides in Escherichia coli K12 adhesion and transport, Langmuir 20 (2004) 7736–7746.
[3] C.A. Flemming, R.J. Palmer, A.A. Arrage, H.C. van der Mei, D.C. White, Cell surface physicochemistry alters biofilm development of pseudomonas aeruginosa lipopolysaccharide mutants, Biofouling 13 (1998) 213–231.
[4] Y.A. Knirel, Polysaccharide antigens of Pseudomonas aeruginosa, Crit. Rev. Microbiol. 17 (1990) 273–304.
[5] M.H. Saier, Bacterial and Archaeal Cell Membranes, in: T.M. Schmidt (Ed.), Encyclopedia of Microbiology, 4, Academic Press, Oxford, 2019, pp. 333–347.
[6] M. Caroff, A. Novikov, Lipopolysaccharides: structure, function and bacterial identification, Ocl Oils Fat Crop Li 27 (2020).
[7] Y.A. Knirel, O.V. Bystrova, N.A. Kocharova, U. Zahringer, G.B. Pier, Conserved and variable structural features in the lipopolysaccharide of Pseudomonas aeruginosa, J. Endotoxin Res. 12 (2006) 324–336.
[8] P. Sperandeo, A.M. Martorana, A. Polissi, Lipopolysaccharide Biosynthesis and Transport to the Outer Membrane of Gram-Negative Bacteria, in: A. Kuhn (Ed.), Bacterial Cell Walls and Membranes, Springer International Publishing, Cham, 2019, pp. 9–37.Bacterial Cell Walls and Membranes, Springer, Cham, 2019.
[9] A. Fomsgaard, Antibodies to lipopolysaccharides: some diagnostic and protective aspects, Apmis 98 (1990) 5–38.
[10] J. Palmer, S. Flint, J. Brooks, Bacterial cell attachment, the beginning of a biofilm, J. Ind. Microbiol. Biot. 34 (2007) 577–588.
[11] A. Korenevsky, T.J. Beveridge, The surface physicochemistry and adhesiveness of Shewanella are affected by their surface polysaccharides, Microbiology+ 153 (2007) 1872–1883.
[12] S.A. Makin, T.J. Beveridge, The influence of A-band and B-band lipopolysaccharide on the surface characteristics and adhesion of Pseudomonas aeruginosa to surfaces, Microbiology (Reading) 142 (Pt 2) (1996) 299–307.
[13] F. El-Taboni, E. Caseley, M. Katsikogianni, L. Swanson, T. Swift, M.E. Romero-Gonzalez, Fluorescence spectroscopy analysis of the bacteria-mineral interface: adsorption of lipopolysaccharides to silica and alumina, Langmuir 36 (2020) 1623–1632.
[14] B.A. Jucker, H. Harms, S.J. Hug, A.J.B. Zehnder, Adsorption of bacterial surface polysaccharides on mineral oxides is mediated by hydrogen bonds, Colloid Surf. B 9 (1997) 331–343.
[15] J. Kazzaz, M. Singh, M. Ugozzoli, J. Chesko, E. Soenawan, D.T. O'Hagan, Encapsulation of the immune potentiators MPL and RC529 in PLG microparticles enhances their potency, J. Control Release 110 (2006) 566–573.

[16] S. Demento, E.R. Steenblock, T.M. Fahmy, Biomimetic approaches to modulating the T cell immune response with nano- and micro- particles, Annu Int Conf. IEEE Eng. Med Biol. Soc. 2009 (2009) 1161–1166.
[17] T.H. Abdoel, H.L. Smits, Rapid latex agglutination test for the serodiagnosis of human brucellosis, Diagn. Microbiol Infect. Dis. 57 (2007) 123–128.
[18] J.M. Peula-Garcia, J.A. Molina-Bolivar, J. Velasco, A. Rojas, F. Galisteo-Gonzalez, Interaction of bacterial endotoxine (lipopolysaccharide) with latex particles: application to latex agglutination immunoassays, J. Colloid Interface Sci. 245 (2002) 230–236.
[19] K. Murali, K. Kenesei, Y. Li, K. Demeter, Z. Kornyei, E. Madarasz, Uptake and bio-reactivity of polystyrene nanoparticles is affected by surface modifications, ageing and LPS adsorption: in vitro studies on neural tissue cells, Nanoscale 7 (2015) 4199–4210.
[20] S. Gomez, C. Gamazo, B. San Roman, M. Ferrer, M.L. Sanz, S. Espuelas, J.M. Irache, Allergen immunotherapy with nanoparticles containing lipopolysaccharide from Brucella ovis, Eur. J. Pharm. Biopharm. 70 (2008) 711–717.
[21] S. Gehring, S.H. Gregory, P. Wintermeyer, M. San Martin, C. Aloman, J.R. Wands, Generation and characterization of an immunogenic dendritic cell population, J. Immunol. Methods 332 (2008) 18–30.
[22] P. Prasad, S. Sachan, S. Suman, G. Swayambhu, S. Gupta, Regenerative core-shell nanoparticles for simultaneous removal and detection of endotoxins, Langmuir 34 (2018) 7396–7403.
[23] M. Piazza, M. Colombo, I. Zanoni, F. Granucci, P. Tortora, J. Weiss, T. Gioannini, D. Prosperi, F. Peri, Uniform lipopolysaccharide (LPS)-loaded magnetic nanoparticles for the investigation of LPS-TLR4 signaling, Angew. Chem. Int Ed. Engl. 50 (2011) 622–626.
[24] S. Saraf, S. Jain, R.N. Sahoo, S. Mallick, Lipopolysaccharide derived alginate coated Hepatitis B antigen loaded chitosan nanoparticles for oral mucosal immunization, Int J. Biol. Macromol. 154 (2020) 466–476.
[25] B. Jang, L. Xu, M.S. Moorthy, W. Zhang, L. Zeng, M. Kang, M. Kwak, J. Oh, J.O. Jin, Lipopolysaccharide-coated CuS nanoparticles promoted anti-cancer and anti-metastatic effect by immuno-photothermal therapy, Oncotarget 8 (2017) 105584–105595.
[26] T. Behnke, C. Wurth, E.M. Laux, K. Hoffmann, U. Resch-Genger, Simple strategies towards bright polymer particles via one-step staining procedures, Dyes Pigments 94 (2012) 247–257.
[27] T. Behnke, C. Wurth, K. Hoffmann, M. Hubner, U. Panne, U. Resch-Genger, Encapsulation of hydrophobic dyes in polystyrene micro- and nanoparticles via swelling procedures, J. Fluor. 21 (2011) 937–944.
[28] Hesse R. Unifit 2018: Unifit Scientific Software GmbH; 2018. www.unifit-software.de/.
[29] P. Wagner, M. Hegner, H.J. Guntherodt, G. Semenza, Formation and in-Situ Modification of Monolayers Chemisorbed on Ultraflat Template-Stripped Gold Surfaces, Langmuir 11 (1995) 3867–3875.
[30] A. Labuda, M. Kocun, M. Lysy, T. Walsh, J. Meinhold, T. Proksch, W. Meinhold, C. Anderson, R. Proksch, Calibration of higher eigenmodes of cantilevers, Rev. Sci. Instrum. 87 (2016), 073705.
[31] R. Ruhal, H. Antti, O. Rzhepishevska, N. Boulanger, D.R. Barbero, S.N. Wai, B. E. Uhlin, M. Ramstedt, A multivariate approach to correlate bacterial surface properties to biofilm formation by lipopolysaccharide mutants of Pseudomonas aeruginosa, Colloid Surf. B 127 (2015) 182–191.
[32] N.C. Santos, A.C. Silva, M.A. Castanho, J. Martins-Silva, C. Saldanha, Evaluation of lipopolysaccharide aggregation by light scattering spectroscopy, Chembiochem 4 (2003) 96–100.
[33] J. Sun, J. Ge, W. Liu, X. Wang, Z. Fan, W. Zhao, H. Zhang, P. Wang, S.-T. Lee, A facile assay for direct colorimetric visualization of lipopolysaccharides at low nanomolar level, Nano Res 5 (2012) 486–493.
[34] A.B. Jodar-Reyes, J.L. Ortega-Vinuesa, A. Martin-Rodriguez, Electrokinetic behavior and colloidal stability of polystyrene latex coated with ionic surfactants, J. Colloid Interface Sci. 297 (2006) 170–181.
[35] M.J. Garcia-Salinas, M.S. Romero-Cano, F.J. de las Nieves, Zeta potential study of a polystyrene latex with variable surface charge: influence on the electroviscous coefficient, Prog. Coll. Pol. Sci. S 115 (2000) 112–116.
[36] A.M. Baty, P.A. Suci, B.J. Tyler, G.G. Geesey, Investigation of mussel adhesive protein adsorption on polystyrene and poly(octadecyl methacrylate) using angle dependent XPS, ATR-FTIR, and AFM, J. Colloid Interface Sci. 177 (1996) 307–315.
[37] A. Dazzi, R. Prazeres, E. Glotin, J.M. Ortega, Local infrared microspectroscopy with subwavelength spatial resolution with an atomic force microscope tip used as a photothermal sensor, Opt. Lett. 30 (2005) 2388–2390.
[38] A. Dazzi, SUB-100-nanometer infrared spectroscopy and imaging based on a near-field photothermal technique ("PTIR"), Biomed. Vib. Spectrosc. (2008) 291–313.
[39] D. Naumann, C. Schultz, A. Sabisch, M. Kastowsky, H. Labischinski, New Insights into the phase-behavior of a complex anionic amphiphile - architecture and dynamics of bacterial deep rough lipopolysaccharide membranes as seen by Ftir, X-ray, and molecular modeling techniques, J. Mol. Struct. 214 (1989) 213–246.
[40] J. Kiwi, V. Nadtochenko, Evidence for the mechanism of photocatalytic degradation of the bacterial wall membrane at the TiO2 interface by ATR-FTIR and laser kinetic spectroscopy, Langmuir 21 (2005) 4631–4641.
[41] A.A. Bhutto, D. Vesely, B.J. Gabrys, Miscibility and interactions in polystyrene and sodium sulfonated polystyrene with poly(vinyl methyl ether) PVME blends. Part II. FTIR, Polymer 44 (2003) 6627–6631.
[42] R.R. Skelly, P. Munkenbeck, D.C. Morrison, Stimulation of T-independent antibody-responses by hapten-lipopolysaccharides without repeating polymeric structure, Infect. Immun. 23 (1979) 287–293.
[43] J.S. Lam, V.L. Taylor, S.T. Islam, Y. Hao, D. Kocincova, Genetic and functional diversity of pseudomonas aeruginosa lipopolysaccharide, Front Microbiol 2 (2011) 118.